

Ni_3TeO_6 —a collinear antiferromagnet with ferromagnetic honeycomb planes

This content has been downloaded from IOPscience. Please scroll down to see the full text.

2010 *J. Phys.: Condens. Matter* 22 056002

(<http://iopscience.iop.org/0953-8984/22/5/056002>)

[View the table of contents for this issue](#), or go to the [journal homepage](#) for more

Download details:

IP Address: 128.178.131.113

This content was downloaded on 16/08/2015 at 10:45

Please note that [terms and conditions apply](#).

Ni₃TeO₆—a collinear antiferromagnet with ferromagnetic honeycomb planes

I Živković^{1,2}, K Prša³, O Zaharko³ and H Berger⁴

¹ Institute of Physics, Bijenička c. 46, HR-10000 Zagreb, Croatia

² Laboratory for Quantum Magnetism, EPFL, CH-1015 Lausanne, Switzerland

³ Laboratory for Neutron Scattering, ETH Zürich and PSI, CH-5232 Villigen-PSI, Switzerland

⁴ Institut de Physique de la Matière Complexe, EPFL, CH-1015 Lausanne, Switzerland

E-mail: zivkovic@ifs.hr

Received 14 October 2009, in final form 14 December 2009

Published 15 January 2010

Online at stacks.iop.org/JPhysCM/22/056002

Abstract

We report a comprehensive study of magnetic properties of Ni₃TeO₆. The system crystallizes in a noncentrosymmetric rhombohedral lattice, space group R3. There are three differently coordinated Ni atoms in the unit cell. Two of them form an almost planar honeycomb lattice, while the third one is placed between the layers. Magnetization and specific heat measurements revealed a single magnetic ordering at $T_N = 52$ K. Below T_N the susceptibility with the magnetic field parallel to the c axis drops towards zero while the perpendicular susceptibility remains constant, a characteristic of antiferromagnetic materials. Neutron diffraction confirmed that the system is antiferromagnet below T_N with ferromagnetic ab planes stacked antiferromagnetically along the c axis. All Ni moments are in the $S = 1$ spin state and point along the c axis.

(Some figures in this article are in colour only in the electronic version)

1. Introduction

Investigations of simple ferromagnets (FMs) and antiferromagnets (AFMs) flourished in the 1960s and 1970s. With both theoretical and experimental advances a rather comprehensive knowledge has accumulated and is now a part of the textbooks. It is often used in a description of more complicated systems in an effort to approach the complexities from the well-known ground.

The recent hot topic in magnetism is spiral antiferromagnetic multiferroics [1]. In the noncentrosymmetric crystal structures incommensurate order may be induced by symmetry allowed Dzyaloshinskii–Moriya interactions, and, provided there is enough coupling between the magnetic and lattice degrees of freedom, one may find multiferroicity. Therefore, inspection of the crystal lattice and possible interactions is an invaluable tool in the search for new materials with interesting properties.

Recently, the reinvestigation of the crystal structure of trinickel tellurium hexaoxide Ni₃TeO₆ has been reported [2]. It improved the crystal lattice parameters established in the initial report by Newnham and Meagher [3]. Little has been done since the original paper on the characterization of the magnetic

properties of Ni₃TeO₆ with the only result published by Zupan and colleagues [4]. Using the ESR technique on the powdered sample they measured the associated g factor to be 2.26, similar to other Ni²⁺ compounds [5, 6]. Their temperature interval was restricted to above 100 K where no sign of a magnetic ordering has been observed. From the Curie–Weiss (CW) behaviour they obtained the Curie temperature $\theta = -34$ K, indicating that the system is AFM.

Given the fact that Ni₃TeO₆ lacks a centre of inversion, we thought that, if the anisotropy of Ni ions is such that in the ordered state the moments are oriented parallel to the plane, it would produce chirality and possibly a (ferro)electric response. However, the measurements of the dielectric constant have not revealed any signature of the (ferro)electricity.

Here we present the detailed investigation of the basic magnetic properties of Ni₃TeO₆ using the neutron diffraction, magnetization and specific heat measurements on powdered and single-crystal samples. We have determined that the system enters the ordered AFM state below $T_N = 52$ K with magnetic moments pointing along the c axis. The magnetic sublattice consists of ferromagnetic honeycomb planes with alternating spin direction along the c axis. The magnetization and specific heat measurements in dc magnetic fields parallel

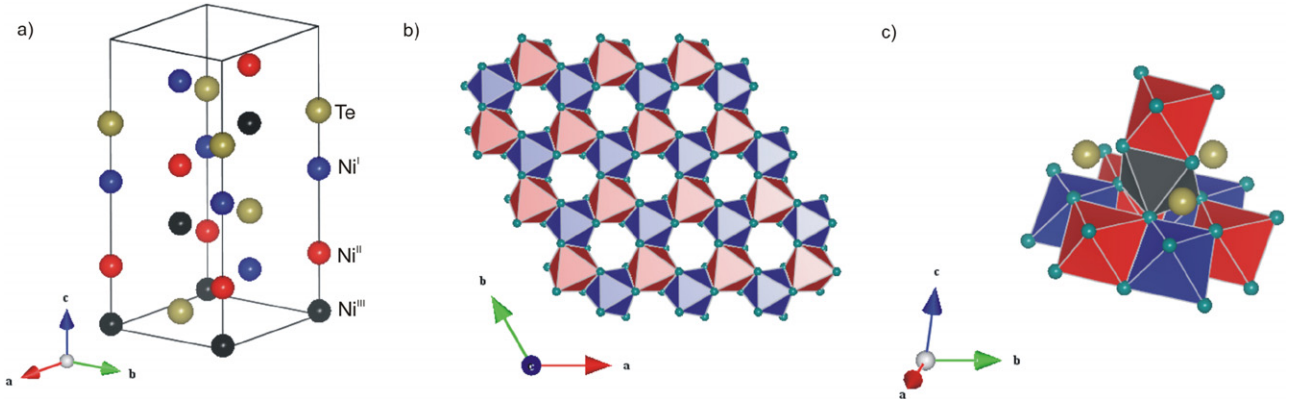


Figure 1. Different views of the structure of Ni_3TeO_6 : (a) the unit cell (oxygen ions are removed for clarity, Ni^{III} placed at the origin), (b) the view along the c axis on the ab plane with its hexagonal structure and (c) the link between the $\text{Ni}^{\text{I}}\text{--}\text{Ni}^{\text{II}}$ hexagon (blue and red) and the Ni^{III} octahedron (black) along the c axis. Ni^{II} ion (red octahedron) on top of Ni^{III} belongs to the adjacent plane.

and perpendicular to the easy axis revealed that Ni_3TeO_6 behaves similar to other canonical AFM compounds.

2. Experimental details

Single crystals of the compound Ni_3TeO_6 were synthesized via chemical vapour transport reactions. The starting materials were NiO (Alfa Aesar 99%), CuO (Alfa Aesar 99.99%), TeO_2 (Acros 99%) and NiCl_2 (Alfa Aesar 99.9%) and the crystals were grown from the non-stoichiometric molar ratio $\text{NiO}:\text{CuO}:\text{TeO}_2:\text{NiCl}_2 = 4:1:3:1$. The starting powder was mixed in an agate mortar and placed in a quartz ampoule, which was evacuated to 10^{-5} Torr and sealed. The ampoule was heated slowly to $700\text{ }^\circ\text{C}$ in a tube furnace and held there for four days followed by slow cooling ($50\text{ }^\circ\text{C h}^{-1}$) to room temperature. The sintered powder was dark green and polyphasic and its phase composition was not analysed. About 20 g of this polyphasic powder mixture was placed in a silica tube, which subsequently was evacuated (10^{-5} Torr), and electronic grade HCl was added in sufficient quantity to be used as a transport agent. The ampoule was placed in a two-zone gradient furnace between $750\text{--}600\text{ }^\circ\text{C}$ and after ten weeks two different compounds were observed as single crystals.

- (i) In the centre of the ampoule cubic crystals with a maximum size of $5 \times 5 \times 5\text{ mm}^{-3}$ of dark green Cu-doped $[\text{Ni}_{30}\text{Te}_{32}\text{O}_{90}\text{C}_{12.67}][\text{Ni}_{4.48}\text{Cl}_{15.78}]$ [7].
- (ii) A number of triclinic plates with a maximum size of $6 \times 6 \times 1\text{ mm}^{-3}$ of dark green Ni_3TeO_6 formed at the cold end.

The obtained samples of Ni_3TeO_6 were checked to ensure that they have no appreciable amount of impurity phases by powder x-ray and neutron measurements (below the detection limit). Also, no paramagnetic Curie-like contributions in dc magnetization at low temperature have been observed, even at higher fields, indicating the purity of the crystal.

Magnetization measurements were performed using a Quantum Design superconducting quantum interference device (SQUID) magnetometer in the temperature range $2\text{--}300\text{ K}$ and with fields up to 5 T. The search for the spin-flop

transition was performed on a Quantum Design PPMS system up to 9 T. Specific heat was measured using a Quantum Design PPMS system with a relaxation technique in fields up to 9 T. Neutron powder diffraction data have been collected from a 5 g polycrystalline sample loaded in a vanadium can (diameter 8 mm) with a neutron wavelength of 2.566 \AA in the temperature range $3.35\text{--}60\text{ K}$ on the DMC diffractometer at SINQ, Paul Scherrer Institute, Villigen, Switzerland.

The visualization software VESTA [8] has been used for displaying the crystal structure.

3. Results and discussion

A refinement of the crystal structure performed on the powder sample of Ni_3TeO_6 confirmed the model suggested before [3]. Here we recapitulate the main features which are important for the description of the magnetic behaviour of the compound. Ni_3TeO_6 crystallizes in a rhombohedral lattice, space group $\text{R}3$ (no. 146). The unit cell parameters are $a = 5.103(2)\text{ \AA}$ and $c = 13.755(10)\text{ \AA}$ with Ni atoms occupying the $(0, 0, z)$ positions ($z_{\text{I}} = 0.352$, $z_{\text{II}} = 0.648$, $z_{\text{III}} = 0.852$). Each Ni ion is surrounded by six oxygen ions that form a slightly distorted octahedron. The ligand environment is similar for all three Ni positions, although they differ in the coordination number.

As can be seen from figure 1(a), Te and Ni ions are stacked along the c axis in a regular fashion forming the columns $\text{Te}\text{--}\text{Ni}^{\text{I}}\text{--}\text{Ni}^{\text{II}}\text{--}\text{Ni}^{\text{III}}$. The nonmagnetic Te ion creates holes in the magnetic sublattice, thus preventing the direct magnetic exchange between Ni^{III} and Ni^{I} moments.

Horizontally, Ni^{I} and Ni^{II} ions are connected through two oxygen ions and form an almost planar honeycomb lattice of edge-sharing octahedra (figure 1(b)). Ni^{I} and Ni^{II} ions are shifted slightly with respect to the plane in opposite directions. The $\text{Ni}^{\text{II}}\text{--O--Ni}^{\text{II}}$ angles are 94.1° , suggesting the FM in-plane coupling (J_1).

Each Ni^{II} ion is directly linked with one Ni^{III} ion along the c axis (figure 1(c)). There are three oxygens in between, all forming an angle $\text{Ni}^{\text{II}}\text{--O--Ni}^{\text{III}} = 83.9^\circ$, again indicating the FM interaction (J_2). Two neighbouring planes are shifted relative to each other by $(\frac{a}{3}, \frac{a}{3})$ so that each Ni^{III} ion is

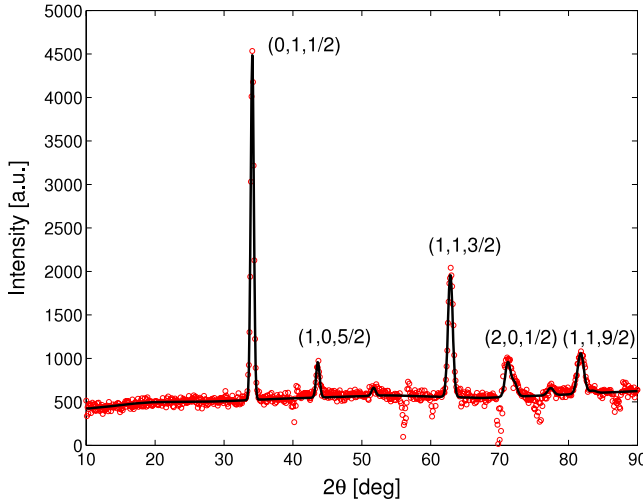


Figure 2. Observed (red dots), calculated (black line) and difference (blue line) neutron powder diffraction pattern of Ni_3TeO_6 at 3.25–60 K.

Table 1. A summary of superexchange interactions in Ni_3TeO_6 . d (Å–B) is the distance in Å between ions A and B. N is the number of superexchange connections between the pair of nickel ions.

| Interaction | Atoms | d (Ni–Ni) | Angle (deg) | N | d (Ni–O) |
|-------------|---|-------------|-------------|-----|------------|
| J_1 (FM) | $\text{Ni}^{\text{I}}\text{--Ni}^{\text{II}}$ | 2.99 | 94.1 | 2 | 1.99, 2.1 |
| J_2 (FM) | $\text{Ni}^{\text{II}}\text{--Ni}^{\text{III}}$ | 2.81 | 83.9 | 3 | 2.1, 2.1 |
| J_3 (AFM) | $\text{Ni}^{\text{III}}\text{--Ni}^{\text{II}}$ | 3.44 | 120.2 | 1 | 1.99, 1.99 |
| J_4 (AFM) | $\text{Ni}^{\text{III}}\text{--Ni}^{\text{I}}$ | 3.73 | 132.1 | 1 | 1.99, 2.1 |

Table 2. The Fourier coefficients of magnetic moments allowed according to the irreducible representations.

| Site | Γ_1 | Γ_2 | Γ_3 |
|--------------------------|-------------|--|---|
| Ni^{I} | $(0, 0, u)$ | $(\frac{3-i\sqrt{3}}{2}u, -i\sqrt{3}u, 0)$ | $(\frac{3+i\sqrt{3}}{2}u, i\sqrt{3}u, 0)$ |
| Ni^{II} | $(0, 0, v)$ | $(\frac{3-i\sqrt{3}}{2}v, -i\sqrt{3}v, 0)$ | $(\frac{3+i\sqrt{3}}{2}v, i\sqrt{3}v, 0)$ |
| Ni^{III} | $(0, 0, w)$ | $(\frac{3-i\sqrt{3}}{2}w, -i\sqrt{3}w, 0)$ | $(\frac{3+i\sqrt{3}}{2}w, i\sqrt{3}w, 0)$ |

positioned above the centre of the hexagon formed by Ni^{I} and Ni^{II} octahedra. There are two different angles between Ni^{III} and the members of the hexagon, $\text{Ni}^{\text{III}}\text{--O--Ni}^{\text{II}} = 120.2^\circ$ (J_3) and $\text{Ni}^{\text{III}}\text{--O--Ni}^{\text{I}} = 132.1^\circ$ (J_4) which indicates that the inter-plane coupling should be AFM. However, the latter interaction also occurs between the Ni^{III} and Ni^{I} of the same spin orientation and may lead to frustration (FM–FM–AFM triangles) in this material. We summarize all the anticipated interactions in table 1.

All the observed peaks in the diffraction pattern could be indexed with the commensurate magnetic wavevector $\vec{k} = (0, 0, 1/2)$. The symmetry analysis for this wavevector reveals that the magnetic representation for all three Ni^{2+} sites can be decomposed into three irreducible one-dimensional representations as $\Gamma = \Gamma_1 \oplus \Gamma_2 \oplus \Gamma_3$, summarized in table 2. Clearly, only the magnetic structures corresponding to irreducible representations Γ_1 (giving all the moments along c) and $\Gamma_2 \oplus \Gamma_3$ (giving all the moments in the ab plane) are

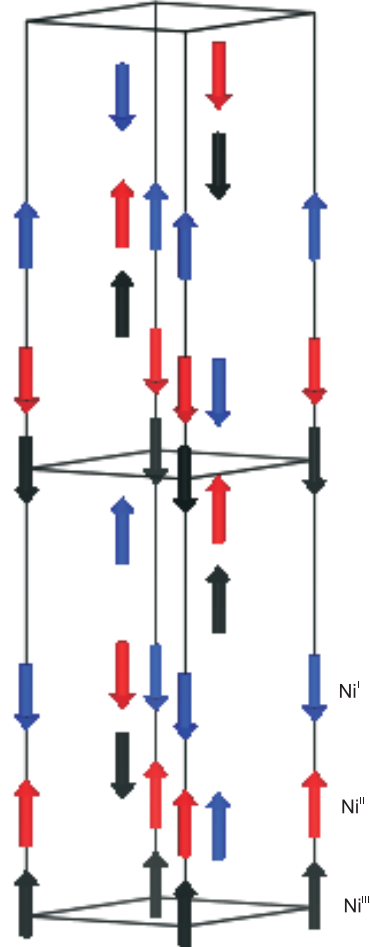


Figure 3. The magnetic structure of Ni_3TeO_6 deduced from the neutron powder diffraction. Arrows denote magnetic moments on particular nickel sites: Ni^{I} —blue, Ni^{II} —red and Ni^{III} —black.

possible. Only the symmetry-adapted mode belonging to Γ_1 fits the experimental data.

In figure 2 we show the low temperature diffraction pattern, alongside the calculated profile for the magnetic structure presented in figure 3. A rather good match was obtained by assuming that the magnetic moments on all Ni^{2+} ions are equal. This assumption is justified by the fact that, although they do not have identical cation neighbours, their ligand environment (six oxygen ions) is similar. The refinement ($R_F = 8.83\%$) gave the value of $2.03(2)\mu_{\text{B}}/\text{ion}$, in accord with the spin value of $S = 1$ for Ni^{2+} ions.

The obtained magnetic structure is in excellent agreement with the conclusions drawn from the angles between the magnetic ions. ab planes are ferromagnetic as well as the coupling between Ni^{II} and Ni^{III} moments which sit on top of each other. The overall antiferromagnetic ground state is the result of the AFM interaction between Ni^{III} and the ferromagnetically coupled hexagon formed by three Ni^{I} and three Ni^{II} moments. We conclude that the antiferromagnetic J_4 exchange interaction is not strong enough to cause the incommensurability of this magnetic structure.

Specific heat has been measured with a dc magnetic field parallel and perpendicular to the c axis. In figure 4 we show

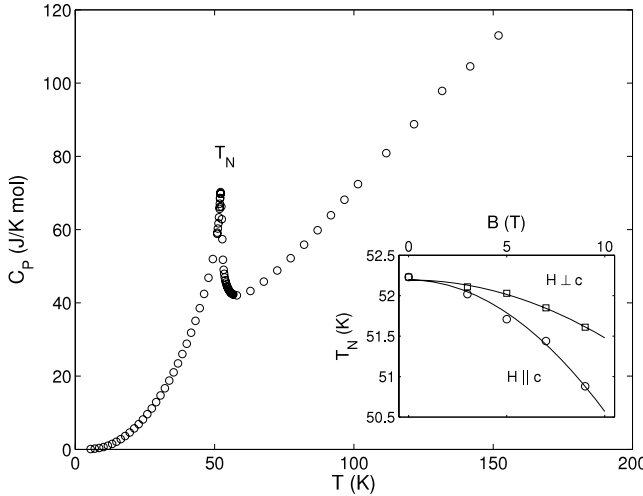


Figure 4. The temperature dependence of the specific heat of Ni_3TeO_6 . The inset shows the field dependence of the transition temperature T_N for the parallel and the perpendicular configuration. Solid lines represent fits to the quadratic dependence (see the text).

the temperature dependence of the specific heat in $H = 0$ T. Around 52 K there is a λ -like feature which marks the transition into a magnetically ordered state. When measured in the applied magnetic field, the transition shifts towards lower temperatures, as indicated in the inset of figure 4. The shift is well reproduced by the quadratic dependence on the field:

$$\delta T = T_N(H) - T_N(H = 0) = -\alpha H^2 \quad (1)$$

where $T_N(H = 0) = 52.20 \pm 0.01$ K is the temperature where C_P has the maximum for zero field. In a simple molecular field approximation (MFA), the quadratic dependence was found for a uniaxial antiferromagnet [14] with a ratio $\alpha_{\parallel}/\alpha_{\perp} \approx 3$. From our measurements we find $\alpha_{\parallel} = 0.0163 \text{ K T}^{-1}$ and $\alpha_{\perp} = 0.0071 \text{ K T}^{-1}$, giving a ratio $\alpha_{\parallel}/\alpha_{\perp} = 2.3$, fairly close to the MFA prediction.

The temperature dependence of the dc susceptibility $\chi_{DC} = M/H$ for two orthogonal field directions is shown in figure 5. At high temperatures both curves nicely follow the CW behaviour $\chi = C/(T + \theta)$, where C is the Curie constant and θ is the Weiss temperature. Around 52 K the system orders and two curves show substantially different temperature dependences. For $H \parallel c$ the susceptibility drops quickly towards zero as the temperature is decreased. On the other hand, the $H \perp c$ curve initially drops down but levels off at low temperature, with a small minimum around 25 K. All these features are well-known characteristics of antiferromagnetic materials with moments pointing along the c axis, in agreement with the magnetic structure deduced from neutron diffraction.

Fitting the measured susceptibility above 150 K to the CW law, we obtain slightly different values for two field orientations: $C_{\parallel} = 1.599 \text{ emu K mol}^{-1}$, $\theta_{\parallel} = 56.1$ K and $C_{\perp} = 1.545 \text{ emu K mol}^{-1}$, $\theta_{\perp} = 51.6$ K. This is not unusual for antiferromagnetic compounds and has been explained in the case of MnF_2 to be due to the long-range dipole–dipole interaction [9, 10].

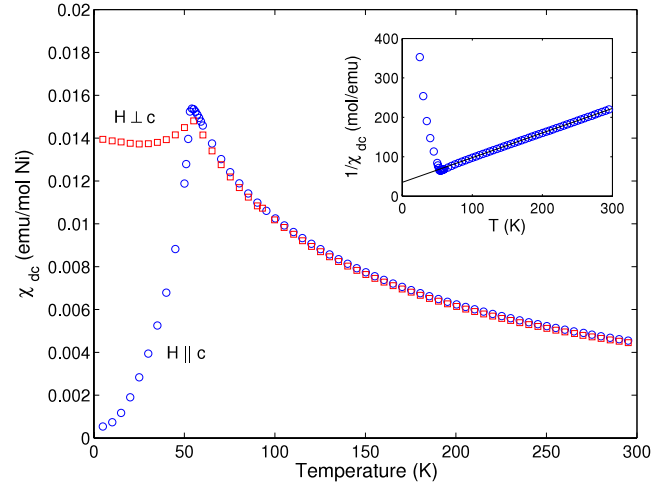


Figure 5. The temperature dependence of the dc susceptibility of Ni_3TeO_6 for the parallel and the perpendicular configuration with $H = 1000$ Oe. The inverse susceptibility for $H \parallel c$ with the Curie–Weiss fit is shown in the inset.

In this fit we have disregarded the temperature-independent contributions, namely the positive Van Vleck (χ_{vv}) and the negative diamagnetic susceptibility (χ_d). χ_{vv} can be calculated from

$$\chi_{vv} = \frac{8\mu_B N_A}{\Delta} = 5.2 \times 10^{-7} \text{ emu mol}^{-1} \quad (2)$$

where μ_B is the Bohr magneton, N_A is the Avogadro number and $\Delta = 10000 \text{ cm}^{-1}$ is the energy gap between the octahedrally split t_{2g} and e_g levels measured by ESR [4]. The diamagnetic susceptibility is [11] $\chi_d = -1.2 \times 10^{-4} \text{ emu mol}^{-1}$, more than two orders of magnitude smaller than the measured value at 300 K. Both contributions can be neglected in the first approximation.

The values for the Weiss constants are in accordance with the observed transition around 52 K, indicating no frustration present in this material and, therefore, $J_4 \ll J_3$. From the Curie constant we can calculate the effective magnetic moment $\mu_{\text{eff}} = 3.58\mu_B$ in the case of the field parallel to the c axis. This is somewhat larger than the theoretically predicted value for the $S = 1$ system $\mu_{\text{eff}}^{\text{calc}} = 3.2\mu_B$ calculated using the measured value [4] $g = 2.26$.

Knowing the exact temperature dependence of the parallel and the perpendicular susceptibilities below T_N one can in principle calculate the values of the exchange constant(s) using Kubo's spin wave theory [12]. However, it has been shown [13] that there are large discrepancies between the experimental values and the theoretical predictions (up to 20%), even for a simple system as MnF_2 .

The modelling of Ni_3TeO_6 is even more complicated by the fact that there are at least three different coupling constants to be considered:

- in-plane J_1 between Ni^{I} and Ni^{II} (FM);
- out-of-plane J_2 between Ni^{II} and Ni^{III} which sit on top of each other (FM);
- out-of-plane J_3 between Ni^{III} and the in-plane hexagon.

In addition to that, the anisotropy constant K is unknown at present, although it should be equal for all the moments (at least in the first approximation). Finally, each nickel ion has a different coordination number z .

Given the fact that our measurements were done with the error in the alignment of the crystal axes with respect to the direction of the magnetic field no better than 5° , we find that the modelling would not be reliable and leave the determination of the exchange constants for future inelastic neutron scattering experiments.

Measuring the magnetization up to 9 T with the magnetic field parallel to the c axis we have not observed the transition to a spin-flop state. In simple AFMs, when the dc magnetic field is applied parallel to the easy axis, above the characteristic field H_{SF} moments are perpendicular to the easy axis but still retain the antiparallel configuration. The magnitude of H_{SF} depends on the anisotropy energy and the exchange energy, $\sqrt{2H_{\text{A}}H_{\text{E}}}$. In Ni_3TeO_6 , given the fact that there are at least three different J s, there is a possibility that more than one characteristic field is present for $H \parallel c$. Studies in larger magnetic fields would be desirable to elucidate this issue.

4. Conclusions

We have presented the results of the investigation of the magnetic properties of Ni_3TeO_6 . This material shows a single magnetic transition at $T_{\text{N}} = 52$ K with a well-defined λ anomaly in the specific heat. Although the crystal structure indicates some magnetic frustration, below T_{N} the system is a collinear antiferromagnet with ferromagnetically ordered ab honeycomb planes. The parallel and perpendicular susceptibilities below T_{N} display a canonical AFM behaviour with χ_{\parallel} reducing to zero for $T \rightarrow 0$ K. The spin-flop transition has not been observed up to 9 T. The preliminary dielectric

constant $\epsilon_r(T)$ measurements down to 10 K do not show any features indicative of a dielectric transition.

Acknowledgments

We gratefully acknowledge T Ivec for the experimental input. This work has been supported by the Croatian Ministry of Science, Education and Sports, project no. 0035-0352843-2845 and the Swiss National Science Foundation, SCOPES project no. 111105. The sample preparation was supported by the NCCR research pool MaNEP of the Swiss NSF. This work was partially performed at SINQ, Paul Scherrer Institute, Villigen, Switzerland.

References

- [1] Cheong S V and Mostovoy M 2007 *Nat. Mater.* **6** 13
Khomskii D 2009 *Physics* **2** 20
- [2] Becker R and Berger H 2006 *Acta Crystallogr. E* **62** i222
- [3] Newnham R E and Meagher E P 1967 *Mater. Res. Bull.* **2** 549
- [4] Zupan J, Kolar D and Urbanc V 1971 *Mater. Res. Bull.* **6** 1353
- [5] Richards P L 1965 *Phys. Rev.* **138** A1769
- [6] Yamaguchi H, Katsumata K, Hagiwara M, Tokunaga M, Liu H L, Zibold A, Tanner D B and Wang Y J 1999 *Phys. Rev. B* **59** 6021
- [7] Johnsson M, Lidin S, Törnroos K W, Bürgi H-B and Millet P 2004 *Angew. Chem.* **116** 4392
- [8] Momma K and Izumi F 2008 *J. Appl. Crystallogr.* **41** 653
- [9] Okazaki A, Turberfield K C and Stevenson R W H 1964 *Phys. Lett.* **8** 9
- [10] Nordblad P, Lundgren L, Figueroa E, Gäfvert U and Beckman O 1979 *Phys. Scr.* **20** 105
- [11] Selwood P W 1956 *Magnetochemistry* (New York: Interscience)
- [12] Kubo R 1952 *Phys. Rev.* **87** 568
- [13] Trapp C and Stout J W 1963 *Phys. Rev. Lett.* **10** 157
- [14] Heller P 1966 *Phys. Rev.* **146** 403